Nuclear Instruments and Methods in Physics Research B 498 (2021) 61–67

Contents lists available at ScienceDirect

Nuclear Inst. and Methods in Physics Research, B

journal homepage: www.elsevier.com/locate/nimb

X-ray dose rate estimation model for an electron linac with thick tungsten target

Pikad Buaphad [a,b,c,*], Yujong Kim [b,c], Kibaek Song [a], Hyung Dal Park [a], Chihyung Kim [c], Seunghyun Lee [c], Hyeri Lee [b,c], Jinsik Ju [c]

[a] KORENS RTX, Gyeryong-si 32842, South Korea
[b] University of Science and Technology (UST), Daejeon 34113, South Korea
[c] Future Light Source R&D Team, Korea Atomic Energy Research Institute, Daejeon 34057, South Korea

ARTICLE INFO

Keywords:
Dose rate estimation
X-ray dose
Bremsstrahlung
Thick-target

ABSTRACT

Recently, there is a strong demand for a high energy, high dose X-ray, which can penetrate thick objects well and provide a good visualization of their inner structures. Normally, such an X-ray can be generated by electron linear accelerators (linacs) with bremsstrahlung. It is necessary to develop a simple formula to estimate the X-ray dose rate from electron linacs. In this paper, we propose a mathematical model to estimate the X-ray dose rate of electron linacs. First, the FLUKA Monte Carlo code has been performed to evaluate the radiation dose due to the bremsstrahlung for different thicknesses of tungsten targets and electron energies. Then, a mathematical model is developed by applying the linear least-squares fitting on the simulated data. It is found that the model is accurate enough to estimate an X-ray dose rate of any electron linacs with a thick tungsten target. A comparison between the simulated and estimated dose rate shows that the mean absolute percentage error is approximately 3%, with the maximum error of 8%. Therefore, this mathematical model could be an alternative way to estimate an X-ray dose rate of an electron linac with a thick tungsten target analytically.

1. Introduction

Since Rontgen discovered the X-ray in 1895, X-ray testing has become a standard technique to identify the inner structure of a test object [1,2]. This technique is widely used in medical, industry, security, and scientific research applications. Each of these applications requires particular conditions such as a specific X-ray energy, a specific radiation dose, and an imaging time. It is necessary to develop and optimize the X-ray source for the specific requirements of each application. With rapidly increasing trade and terrorist threats worldwide, cargo inspection has become the most common application of nondestructive X-ray testing within the industrial sector. A cargo inspection system demands a high energy X-ray with high penetration capabilities to evaluate the content of a steel-walled cargo. The X-ray with mega-electronvolt (MeV) energy is appropriate for this purpose [3]. It can be generated from an electron linear accelerator (linac) through the bremsstrahlung radiation. The useful X-ray energy range for producing the ability to penetrate over 100 mm of steel is 1–20 MeV. In 1990, however, the World Health Organization (WHO) limited the X-ray energy to be below 10 MeV to protect high dose exposure and reduce the radiation shielding material [4]. Therefore, any X-ray applications using X-ray energy higher than 10 MeV must have extensive radiation shielding.

The bremsstrahlung X-ray generated from the electron bombardment of a thick target is a complex process. The bremsstrahlung radiation depends on the cross-section of electron interaction with an atom in the target. When electrons hit the target, they are decelerated and lose energy due to the Coulomb force between the electron beam and the nucleus in the target. Then, the lost kinetic energy is converted into heat and X-ray radiation. A common target used to convert the electron energy into bremsstrahlung X-ray is tungsten because it has a high atomic number and a high melting point. As the energy loss of an electron determines the X-ray energy, the bremsstrahlung X-rays energy is always lower than the electron energy. The X-ray radiation dose is mainly a function of the electron beam energy, the target material, and the target thickness.

The accurate value of the X-ray dose rate produced by electron linac is an important criterion for designing electron linac. Generally, the Monte Carlo method is applied to calculate the X-ray dose rate of

* Corresponding author at: *KORENS RTX*, Gyeryong-si 32842, South Korea.
E-mail address: buappika@irtx.co.kr (P. Buaphad).

https://doi.org/10.1016/j.nimb.2021.04.009
Received 21 August 2020; Received in revised form 6 April 2021; Accepted 8 April 2021
Available online 8 May 2021
0168-583X/

electron linac. However, the Monte Carlo simulation takes a considerable long time to estimate the radiation dose. The time-consuming process of the Monte Carlo simulation brings our study to make a reliable and simple mathematical model to estimate the X-ray dose rate. In this paper, we modeled an electron linac head using the FLUKA Monte Carlo code with FLUKA Advanced Interface (FLAIR). The FLUKA simulation calculates the X-ray dose rate from an electron linac with various tungsten target thicknesses for electron energy between 1 MeV up to 20 MeV. A simple mathematical formula as a function of target thickness and electron energy is derived from the simulated dose data. This formula can easily be used to calculate an X-ray output dose of electron linacs. The limitations of our model are also discussed in this paper.

2. Simulation electron linac head

FLUKA is a multipurpose code for the Monte Carlo simulation of transport and interaction of 60 different particles in the matter, which was initially developed by European Organization for Nuclear Research (CERN) and Italian Institute for Nuclear Physics (INFN) [5]. This code can track electron particle interactions with matter over the energy range from 1 keV to 100 TeV. It is widely used in particle accelerators for dose calculation and radiation energy distribution. Although FLUKA is a Fortran based simulation code, a user-friendly graphical interface for FLUKA, called FLAIR, has been developed using Python. FLAIR provides an integrated development environment for all FLUKA simulation stages from writing input files, code execution, status monitoring, and plot generation [6]. The dose rate simulations in this study were carried out using the FLAIR version 2.3–1 running on the FLUKA version 2020.0. beta.1 code package.

Fig. 1 shows the simplified electron linac head for dose calculation in the FLUKA Monte Carlo code. This linac head working in flattening filter free mode provides an increase in the radiation output. Tungsten with a diameter of 40 mm is used for the X-ray target. The tungsten is placed perpendicular to the electron beam, and its thickness is varied from 0.1 mm to 5 mm. There is a 9° half-angle lead collimator with a 219.4 mm long downstream of the target. Therefore, the bremsstrahlung photon can be emitted only in the forward direction. As the dose values are dependent on the absorber material, frequently, an absorbed dose to water is used as a reference. So in this study, a water detector with a volume of $600 \times 600 \times 10$ mm^3 is used to detect radiation output dose at a Source to Surface Distance (SSD) of 1000 mm downstream of the target. This detector is placed axial and perpendicular to the electron beam. In addition, 1000 mm air has been added between the target and detector to attain experimental conditions. The electron beam with an energy range between 1 MeV and 20 MeV is used as the incident beam in FLUKA simulations. This electron beam has a uniform energy distribution and transverse Gaussian distribution with a full-width half maximum (FWHM) of 2 mm. The radiation source, beam parameter, linac head geometry with their materials, and dose results can be defined in the FLUKA input file. An example of the FLUKA input file to define the electron source and linac head is given in Appendix.

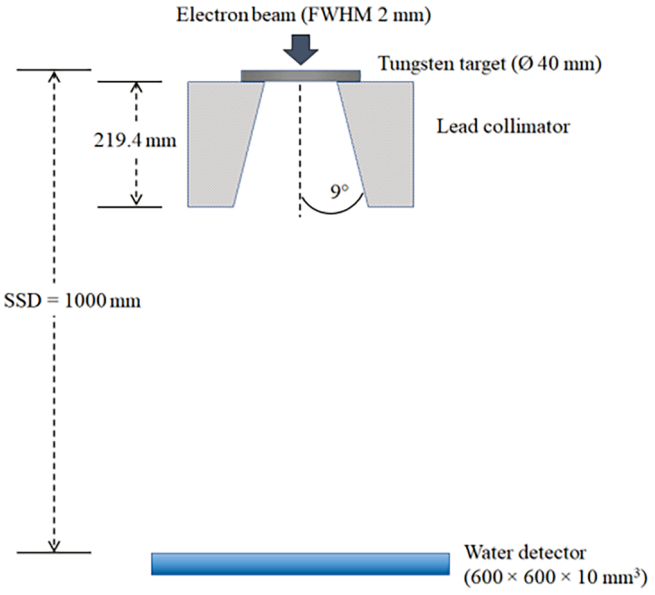

Fig. 1. The schematic of the linear accelerator head and water detector in FLUKA.

In the FLUKA code, there are several options for electron interactions and transport thresholds, called cards. The PRECISIO card is selected as predefined physics settings in the DEFAULTS section. In the biasing section, the cutoff energy 50 keV for electrons and 1 keV for photons are defined by using the EMFCUT card. Moreover, the EMFFIX card is used to define energy loss per step of 10%. The 5×10^7 primary electrons for five cycles are simulated in FLUKA code to keep the statistical uncertainty below 5%. In the output settings section of the FLUKA code, the X-ray dose and X-ray energy distribution can be estimated by using USRBIN and USRBDX scores, respectively. USRBIN calculates the energy stored in the detector, and its results are expressed in GeV/cm^3 per electron unit. Then, USRBIN results must be multiplied by $6 \times 10^7/\rho$ to obtain the doses in Gy μA^{-1} min^{-1} unit. Here, ρ is the detector density in g/cm^3. USRBDX score is used to calculate the X-ray energy distribution passing through a defined surface area in a unit of particle/cm^2 to a forward direction.

3. Thick-target bremsstrahlung formula

We are interested in developing a reasonably simple formula for the MeV X-ray dose as a function of target thickness and electron beam energy. As the incident electron energy high (in MeV order), we can consider only the electron energy loss due to bremsstrahlung and the X-ray attenuation along its path. Kramer was the first person to propose a formula for thick target bremsstrahlung in 1923 [7]. He used a classical method for the interaction of an electron with a target atom. Kramer equation gives the bremsstrahlung radiation intensity as a function of photon energy generated from a target atom of the atomic number of Z at any given incident electron energy E_0 as [7–9]

$$I(E) = \text{constant} \times Z(E_0 - E), \tag{1}$$

where E is the generated X-ray energy. This simple equation explains that the X-ray energy spectrum depends linearly on both the atomic number of a target and electron energy. As the target used to produced X-rays is thick, the incident electrons are much more likely to lose a small proportion of their energy from multiple interactions with the target atom and produce a large number of low energy X-rays. Additionally, the X-ray photon number is zero when $E \geq E_0$. Kramer's theory assumed that the radiation is isotropic angular distribution. However, the bremsstrahlung radiation angular distribution is not isotropic. It depends on the bremsstrahlung differential cross-section.

Suppose the target is thick enough to stop the electron beam within the target. The simple Kramer's equation can be improved by considering that the angular dependence of the X-ray due to multiple elastic scatterings when it travels through the target. Therefore, the X-ray bremsstrahlung spectrum is expressed in terms of the bremsstrahlung differential cross-section and the electrons stopping power in the target. Then, the generated X-rays are attenuated along their paths from the target to the detector. In this study, the X-rays pass through tungsten and air before hit a water detector. In addition, the inverse square law must be included because the X-ray intensity becomes weaker as it spread out from the source. Finally, the generated X-ray photon energies are absorbed to the detector of density of ρ. In general, the X-ray bremsstrahlung output of the industrial electron linac is measured at an angle of 0° to the electron beam at a given SSD. Therefore, the X-ray intensity

spectrum detected at an angle of 0° relative to the electron beam, and the SSD of d from electron energy E_0 is given by

$$I(Z, E_0, E, d) = \text{constant} \times \frac{Z}{d^2} e^{-(\mu_W - \mu_{Air})t} e^{-\mu_{Air} d} \left(\frac{\mu_{en}}{\rho}\right)_{Water} \frac{d\sigma}{dE} \frac{E}{(-dE/dx)}, \quad (2)$$

where t is the tungsten target thickness. μ_W and μ_{Air} are the X-ray attenuation coefficients in tungsten and air, respectively. $(\mu_{en}/\rho)_{Water}$ is the X-ray energy absorption coefficient of the water detector. The X-ray attenuation coefficients and energy absorption coefficients for all materials of electron linac head covering X-ray energies from 1 keV to 20 MeV are available from the National Institute of Standards and Technology (NIST) reference database 126 [10]. $d\sigma/dE$ is the bremsstrahlung differential cross-section from the tabulation of Seltzer and Berger [11]. They published extensive tables for the bremsstrahlung differential cross-section covering electron energies from 1 keV up to 10 GeV incident on neutral atoms with atomic numbers Z from 1 to 100. $-dE/dx$ is the electron stopping power of the incident electron energy E_0 in the tungsten target and can be obtained from the NIST Stopping Powers and Ranges for Electrons (ESTAR) database [12].

Fig. 2 shows the X-ray energy spectra per incident electron from FLUKA simulation and our analytical expression in Eq. (2). These curves represent a sharp dip for low X-ray energy due to the strong X-ray absorption of a target atom. It is observed that the energy distribution of our model is in good agreement with the simulation data, although there are a few areas of difference. To obtain the dose rate from Eq. (2), the electron beam current hitting the target must be taken into account. However, it can be independent of beam current by using dose rate per beam current unit such as Gy μA^{-1} min^{-1}. For generated polyenergetic X-ray radiation, the X-ray dose is to integrate all the X-ray bremsstrahlung energies produced by the electron as it slows down in the thick target as

$$\dot{D} = \text{constant} \times \frac{Z}{d^2} \int_0^{E_0} e^{-(\mu_W - \mu_{Air})t} e^{-\mu_{Air} d} \left(\frac{\mu_{en}}{\rho}\right)_{Water} \frac{d\sigma}{dE} \frac{E}{(-dE/dx)} dE. \quad (3)$$

The integral is taken from zero to the incident electron energy E_0. The integration of $\dot{D}$ in Eq. (3) cannot be directly solved. However, one can easily approximate the analytical form of the Eq. (3) as [13]

$$\dot{D} = k(Z, d) e^{-\alpha t} {E_0}^n \quad (4)$$

where, k is a function of linac head geometry and material of the target. α is a linear combination of attenuation coefficients in all materials along the X-ray path and depends on the incident electron energy. n is the power of incident electron energy. This analytic expression can adequately display results with coefficients of k, α, and n. The ${E_0}^n$ term represents the bremsstrahlung produced at electron energy E_0, and the $e^{-\alpha t}$ factor is the X-ray attenuation in the target thickness t.

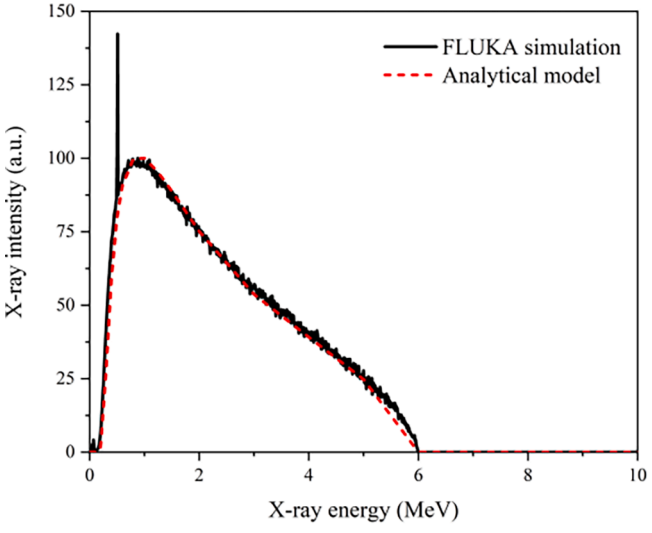

Fig. 2. Analytically calculated and simulated X-ray intensities generated from the 6 MeV electron energy with a tungsten target thickness of 3 mm at SSD of 1000 mm.

4. FLUKA simulation results

The X-ray dose profiles computed by FLUKA were taken through the center values in the x and y directions of the field. Each profile is an average of five simulation cycles to provide better statistics. After FLUKA simulations, the data smoothing method with a 2D median filter in MATLAB code is used to remove noise from the dose profile. Fig. 3 demonstrates the X-ray dose profile of the 60 × 60 mm^2 field produced from electron energy of 6 MeV and tungsten thickness of 3 mm. As these doses were generated from a gaussian beam profile, the output X-rays also have a gaussian profile. In this study, the dose rate used to determine the mathematical model is defined at the maximum value of the profile. Fig. 4 shows the X-ray output dose rate of various tungsten target thicknesses. It is observed that as the target thickness increases, the X-ray dose decreases. Moreover, the dose rate at the thin target has decreased rapidly. Then, this decrease has slowed down at the thick target. The extremely high dose at thin target is due to electron leakage from the target. This transmitted electron can contaminate the X-ray output and generates an extra X-ray photon, which is unwanted in X-ray testing. Generally, electron energy leakage per surface area of 100 mm^2 should be below 0.05%.

Therefore, it is necessary to find the thinnest target for stopping a given incident electron energy within a target. The values of the thinnest target, which can reduce the electron leakage below 0.05% at various electron energies are plotted in Fig. 5. It is understood in Fig. 5 that the minimum target thickness for different electron energy could be well fitted by $t_0 = (0.269 \pm 0.003)\ E_0 + (0.26 \pm 0.03)$ mm. Here, E_0 is an incident electron energy in MeV. This relation can be estimated with a standard deviation of 0.07 mm.

5. Discussion

A mathematical model was developed for modeling the output dose of electron linac. The goal was to build a mathematical model which could estimate the dose rate produced by electron linac at any given electron energy and any given tungsten target thickness. As the model is expressed in Eq. (4), the output X-ray dose is an explicit function of

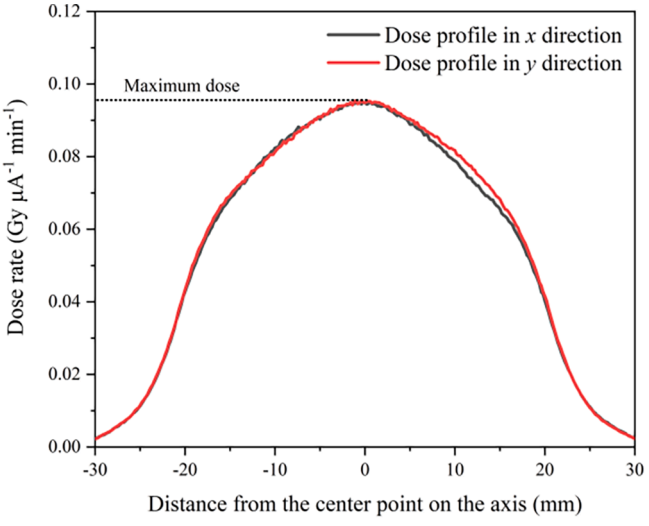

Fig. 3. The dose profile of 60 × 60 mm^2 produced from electron energy of 6 MeV and tungsten target thickness of 3 mm.

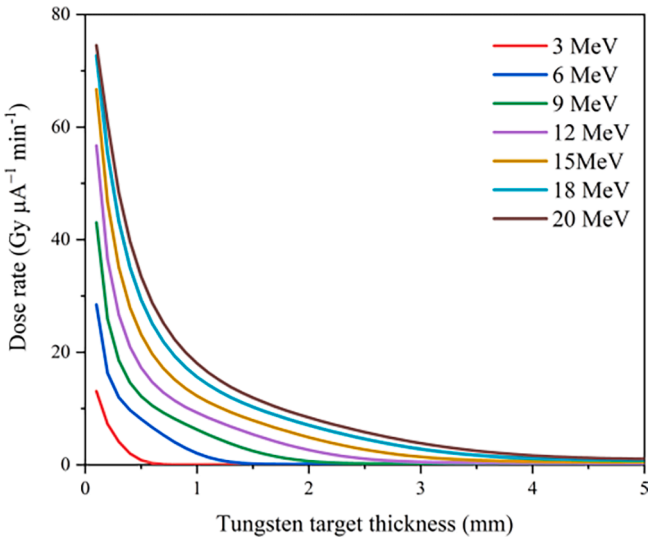

Fig. 4. X-ray output dose rate as a function of tungsten target thickness for different incident electron energies.

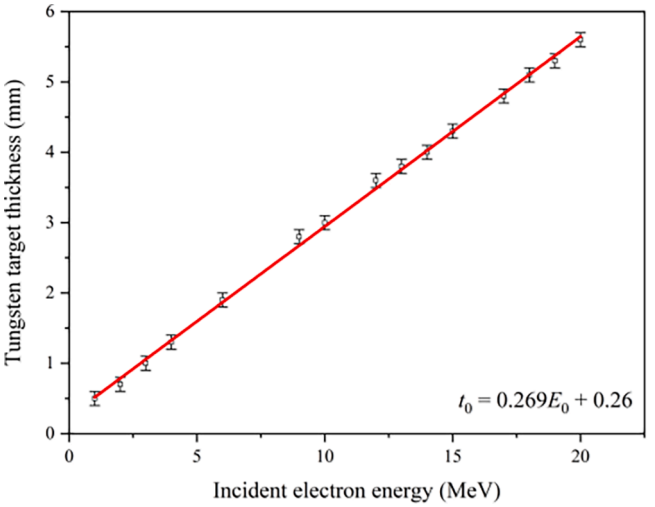

Fig. 5. The minimum thickness of tungsten for various electron energies that can reduce the electron leakage to be lower than 0.05%.

incident electron energy and target thickness. However, the values of the unknown coefficient in Eq. (4) have not been given yet. Thus, in this section, we investigate these unknown coefficients. As the X-ray bremsstrahlung radiation is an anisotropic angular distribution, our mathematical model proposed in this paper will only estimate the X-ray dose at an angle of 0° relative to the electron beam axis with SSD of 1000 mm. The linear least-square method is the best tool to determine the values of parameters k, α, and n in Eq. (4).

5.1. Dose rate due to target thickness

In general, bremsstrahlung X-ray is produced from the electron bombardment of a thick tungsten target. Then, the X-ray photons are exponentially attenuated along their path. Therefore, an increase in the target thickness results in a dose reduction due to self-absorption in materials along the X-ray path. The X-ray self-absorption term can be expressed in the form of $e^{-\alpha t}$. However, the target thickness t must be thicker than t_0 for each given electron energy. The dose rate reduction due to X-ray attenuation for various electron energies and tungsten target thicknesses is shown in Fig. 6. For a given electron energy, the α

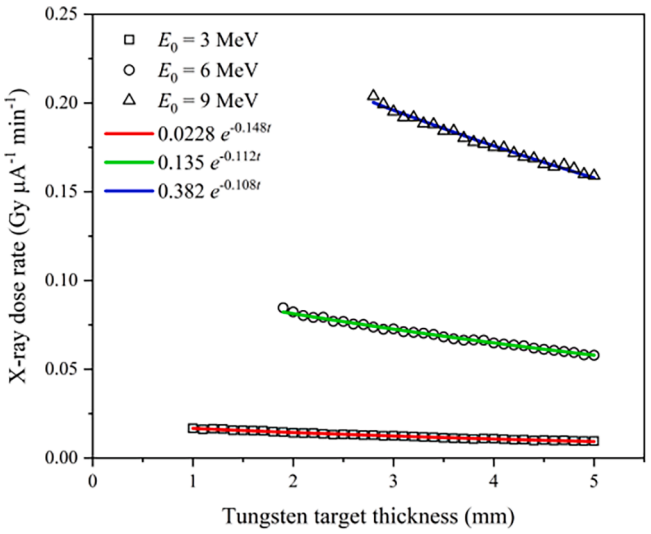

Fig. 6. The dose rate reduction due to X-ray attenuation for different electron energies and tungsten thicknesses.

coefficient value could be obtained by fitting the exponential term to the dose rate data. After fitting the dose rate data, the calculated α coefficients for the electron energy range from 1 MeV to 20 MeV are listed in Table 1 and plotted in Fig. 7. Fig. 7 shows that the α coefficient depends on the incident electron energy. This coefficient decreases substantially from electron energy of 1 MeV to10 MeV, but it changes slightly at higher electron energies. As X-rays were absorbed along their path with the attenuation coefficient of α, therefore, the α coefficient could be expressed in the linear combination of attenuation coefficients of all materials along the X-ray path. For our study, the bremsstrahlung X-rays pass through the tungsten and air along their path. Therefore, the α coefficient in mm^{-1} unit is obtained as

$$\alpha = (0.85 \pm 0.06)\mu_W + (26167 \pm 605)\mu_{Air} - (0.033 \pm 0.004), \quad (5)$$

where μ_W and μ_{Air} are the X-ray attenuation coefficients in tungsten and air in mm^{-1} unit, respectively.

5.2. Dose rate due to electron energy

As mentioned in Section 3, the X-ray dose rate is not only a function of target thickness. It also depends on the incident electron energy. An analytical relationship between incident electron energy and output dose rate is required to obtain a value of parameter n in Eq. (4). First, the

Table 1
The FLUKA simulation data generated from a given electron energy with the thick tungsten target.

E_0 (MeV)	t_0 (mm)	Attenuation coefficient, α (mm^{-1})	Thickness-independent dose rate, $\dot{D}$ (Gy μA^{-1} min^{-1})
1	0.5	0.276 ± 0.006	0.0012 ± 0.0001
2	0.7	0.178 ± 0.003	0.0079 ± 0.0003
3	1.0	0.148 ± 0.002	0.0228 ± 0.0004
4	1.3	0.132 ± 0.002	0.0481 ± 0.0009
6	1.9	0.112 ± 0.001	0.135 ± 0.002
9	2.8	0.108 ± 0.002	0.382 ± 0.003
10	3.0	0.104 ± 0.002	0.489 ± 0.004
12	3.6	0.111 ± 0.003	0.781 ± 0.007
13	3.8	0.116 ± 0.004	0.940 ± 0.009
14	4.0	0.126 ± 0.006	1.13 ± 0.01
15	4.3	0.119 ± 0.007	1.34 ± 0.01
17	4.8	0.108 ± 0.003	1.831 ± 0.008
18	5.1	0.108 ± 0.002	2.091 ± 0.007
19	5.3	0.107 ± 0.004	2.39 ± 0.01
20	5.6	0.117 ± 0.004	2.730 ± 0.005

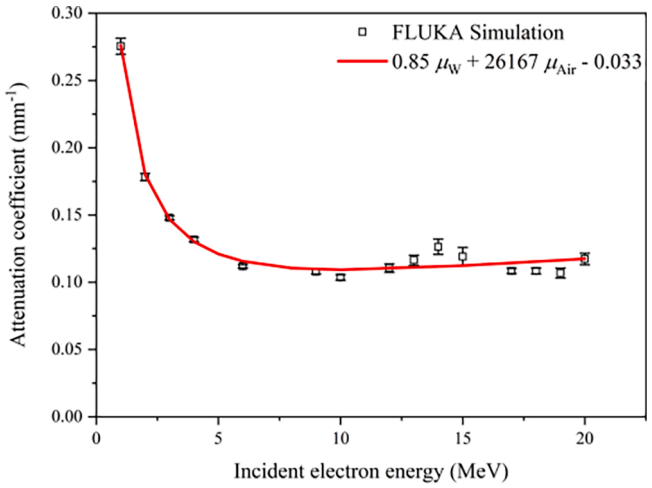

Fig. 7. The calculated α coefficient at different incident electron energies.

X-ray attenuation term must be excluded from the simulated dose rate data to obtain the target thickness independent. For a given electron energy, the target thickness independent bremsstrahlung dose can be obtained by multiplying the simulated dose rate data with $e^{\alpha t}$ term. Then, we average dose rates of all target thicknesses for each given electron energy. Consequently, the dose rates become target thickness independent values and are listed in the Table 1. Fig. 8 plots the target thickness independent dose rate for any given electron energy. The plotted points can be expressed in the $kE_0{}^n$ relation. By using the linear least-squares method, the estimated value of n power is $n = 2.49 \pm 0.01$ for the tungsten target. The calculated n power value for tungsten target is similar to the experimental data of Zhao. Zhao indicated that the typical value of n power varies from 2 to 3 [13].

5.3. Determine k value

Typically, the coefficient k is a function of linac head geometry and target material. In this study, the X-ray dose rates are detected at the angle of 0° relative to the electron beam axis with SSD of 1000 mm. From the thickness-independent dose data, we multiply the data with $E_0^{-2.49}$ term to remove the energy-dependent factor. Then, these data are plotted in Fig. 9. It is observed that the values of k strongly depend on the energy of the incident electrons. According to Eq. (3), however, the k value is an implicit function of the incident electron energy. We found

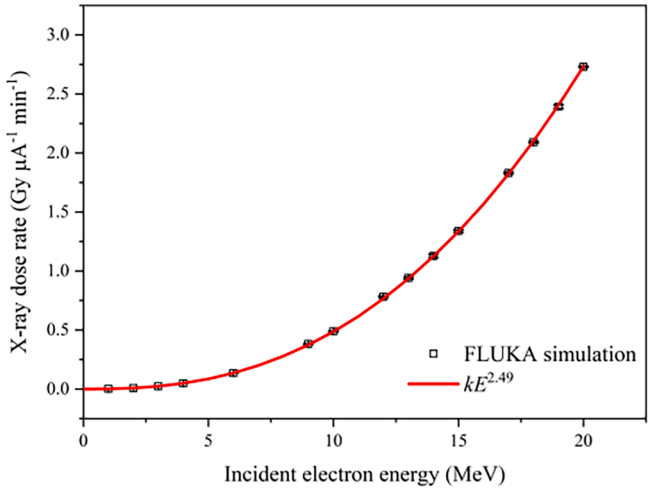

Fig. 8. X-ray thickness-independent dose rate generated from various incident electron energies.

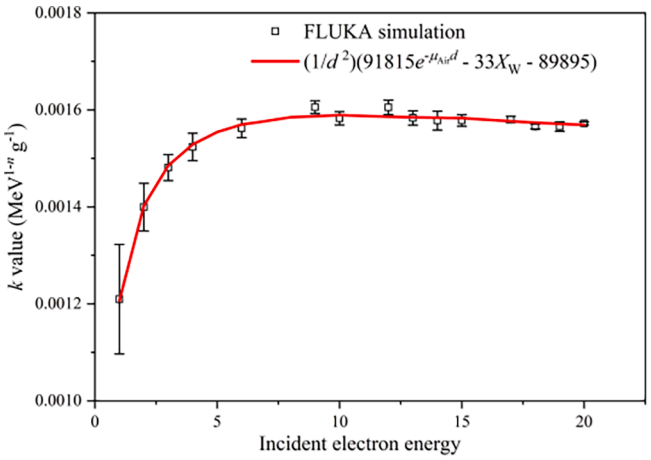

Fig. 9. The k values for each electron energy of the tungsten target.

that the coefficient k can be expressed by linear combining the continuous slowing down approximation (CSDA) range of electrons in the tungsten term and the X-ray attenuation in the air term, μ_{Air}. The electron CSDA range in tungsten target is calculated by following Eq. (6):

$$X_W = \int_0^{E_0} \frac{1}{(-dE/dx)} dE \tag{6}$$

The values of electron CSDA range can also be found in the ESTAR database of NIST [12]. For the X-ray attenuation in the air, it is given in the form of $e^{-\mu_{Air}d}$. Finally, the estimated k value is given in unit of MeV^{1-n} g^{-1} as Eq. (7):

$$k = \frac{1}{d^2}\left((91815 \pm 3392)e^{-\mu_{Air}d} - (33 \pm 3)X_W - (89895 \pm 3371)\right) \tag{7}$$

Here, X_W is the range of electron slowing down in tungsten in mm unit. $d = 1000$ mm is the SSD of our study.

Based on the data analysis method, for a given tungsten target thickness t and electron energy E_0, the X-ray dose rate equation can be expressed as Eq. (8) in Gy μA^{-1} min^{-1} unit:

$$\dot{D} = \frac{1}{d^2}\left(91815e^{-\mu_{Air}d} - 33X_W - 89895\right)e^{-(0.85\mu_W + 26167\mu_{Air} - 0.033)t}E_0{}^{2.49}. \tag{8}$$

5.4. Quantifying model error

In this section, we use a simple method to quantify model discrepancy when fitting data to our mathematical model. The dose rate differences between the FLUKA simulated data and our mathematical model estimated data are visualized as observed residuals. It is evident from the results that there is no massive difference between the simulation results and our model outputs. The mean absolute percentage error of our model is approximately 3%. The lowest mean absolute percentage error is 0.2%, and the highest is 8%. We also found that the mean absolute percentage error at low electron energy is much higher than one at high electron energy.

In this study, the mean of residuals is one of the tools to determine whether our predicted model correctly represents the simulation data. If the mean of residuals is near zero, it indicates that the best fit had been achieved. Moreover, the residual distribution shape of all data sets must follow a normal distribution. In Fig. 10, the scatter plot of standardized residuals is used to check if they have any particular pattern. However, these residuals appear to be randomly scattered around the x-axis without any trend. We also use a boxplot to visualize the residuals based on a five-number summary, as shown in Fig. 10. This shows a median as a horizontal line inside the box at 0.04. A red star dot represents a mean of residual at 0.007. There are a few red diamond dots as outliers occurring outside the 1.5 times

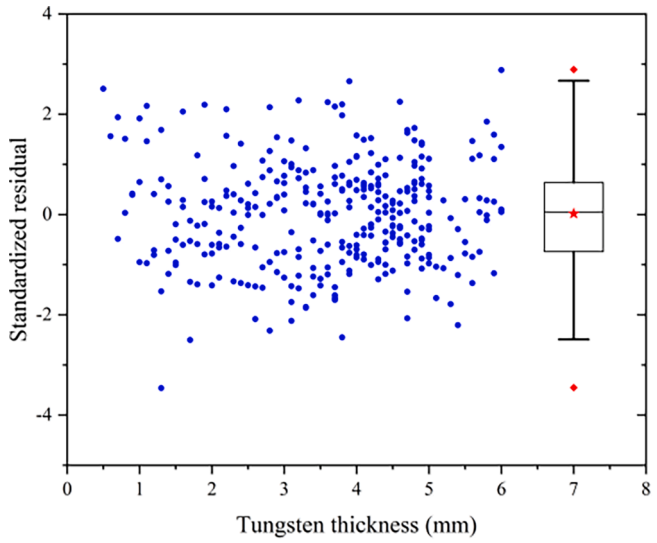

Fig. 10. The scatter plot and boxplot of standardized residuals of our mathematical model.

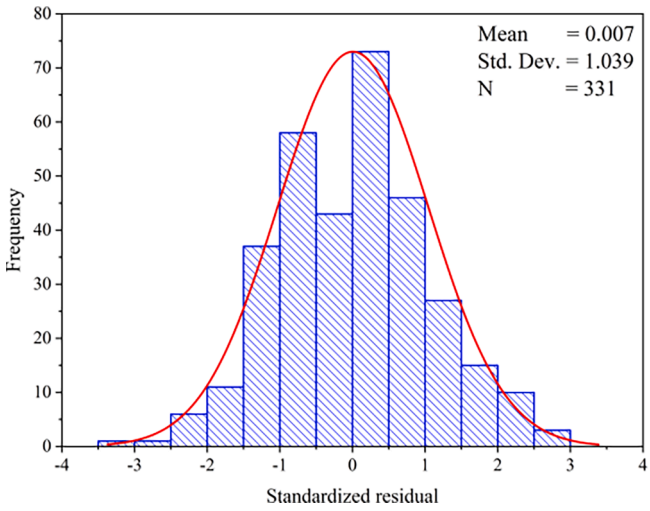

Fig. 11. The histogram of standardized residuals and normal distribution plot.

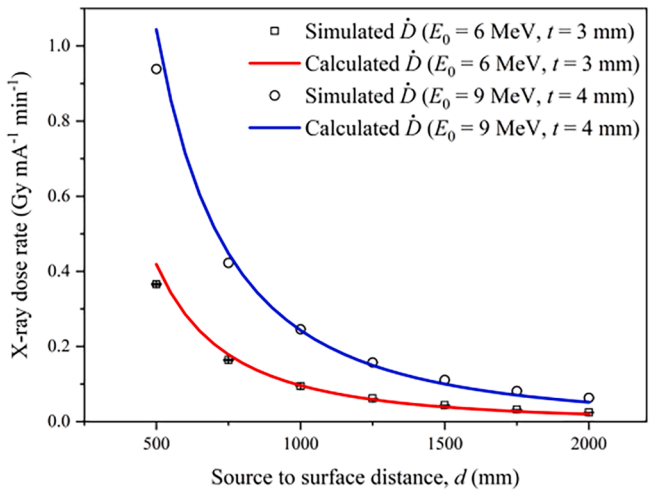

Fig. 12. The simulated and calculated X-ray dose at various SSDs along the center beam axis.

interquartile range (1.5 IQR) from both ends of the box.

The histogram of the standardized residuals of the predicted model is used to visualize our standardized residual distribution, as displayed in Fig. 11. From the data, we estimate the mean of the standardized residual to be 0.007 with a standard deviation of 1.039. Chi-square goodness of fit test was performed to determine whether the normal distribution is a suitable model for our residual distribution at the 5% significance level. As the degree of freedom for χ^2 distribution is 15, we obtain $\chi^2(15, N = 331) = 17.05$, $p = .38$. Therefore, the standardized residuals of our model are consistent with a normal distribution. As shown in Fig. 11, the error residuals of our predicted model have a normal distribution with a good fitting. At the current stage of development of our mathematical model, a good agreement is found between the model and experimental results.

However, this mathematical model is developed based on the X-ray dose rate data at an SSD of 1000 mm. Therefore, the X-ray dose rates at various SSDs along the center beam axis are investigated to validate our estimation model at different SSDs. The simulated X-ray dose rates from various SSDs with the 6 MeV and 9 MeV electron beams are shown in Fig. 12. Our estimated X-ray dose rate results are compared with the FLUKA simulation results to determine our estimated model error. It is found that the mean absolute percentage error increases when an SSD is not 1000 mm. The maximum mean absolute percentage error is approximately 20% for the SSD of 2000 mm. Moreover, this mathematical model has some limitations. First, we have not evaluated the X-ray dose rate from a thin target because there is a high transmitted electron. The tungsten target thickness should be thicker than t_0. This thickness is adequate to stop the electrons in the tungsten target. Second, the effects of the target material on the X-ray dose rate in this formula require further study. This formula is also limited to specific fixed geometry conditions.

6. Conclusion

We have obtained a suitable mathematical model for predicting the X-ray output dose rate from electron linacs with a tungsten target. A wide range of bremsstrahlung dose rate for different electron energies and target thicknesses can be estimated with only three parameters (k, α, n). The value of all parameters can be found by linear least-squares fitting the FLUKA simulation data. A comparison of the results obtained from the model and those from FLUKA simulation shows that the difference between both is quite small with a maximum percentage error of 8%. However, there are some limitations of this mathematical model. As the different target materials were not studied in this paper, it is not possible to comment on the agreement of the mathematical model with the absolute scale of data. Moreover, we can only predict the output X-ray dose rate at an angle of 0° relative to the electron beam axis with an SSD of 1000 mm.

Declaration of Competing Interest

The authors declare that they have no known competing financial interests or personal relationships that could have appeared to influence the work reported in this paper.

Appendix A. Supplementary data

Supplementary data to this article can be found online at https://doi.org/10.1016/j.nimb.2021.04.009.

References

[1] D. Mery, X-ray Testing: The State of the Art, NDT.net Journal. (2013). https://www.ndt.net/article/ndtnet/2013/1_Mery.pdf (accessed August 17, 2020).

[2] A.J. Antolak, Overview of Accelerator Applications for Security and Defense, Rev. Accel Sci. Technol. 08 (2015) 27–36, https://doi.org/10.1142/s1793626815300029.
[3] P.M. Shikhaliev, Megavoltage cargo radiography with dual energy material decomposition, Nucl. Instr. and Meth. in Phys. Res. A 882 (2018) 158–168, https://doi.org/10.1016/j.nima.2017.11.001.
[4] J. Bendahan, Vehicle and cargo scanning for contraband, Physics Procedia 90 (2017) 242–255, https://doi.org/10.1016/j.phpro.2017.09.003.
[5] A. Ferrari, P.R. Sala, A. Fasso, J. Ranft, FLUKA: a multiparticle transport code, (2005), https://dx.doi.org/10.2172/877507.
[6] V. Vlachoudis, FLAIR: a powerful but user friendly graphical interface for FLUKA, Proc. Int. Conf. on Mathematics, Computational Methods & Reactor Physics, Saratoga Springs, New York, (2009), http://www.fluka.org/flair/Flair_MC2009.pdf.
[7] M. Semaan, C.A. Quarles, A model for low-energy thick-target bremsstrahlung produced in a scanning electron microscope, X-Ray Spectrom. 30 (2001) 37–43, https://doi.org/10.1002/xrs.465.
[8] D. Tan, B. Heaton, Bremsstrahlung intensity and spectrum—Theoretical deduction and discussion, Appl. Radiat. Isot. 45 (1994) 1101–1111, https://doi.org/10.1016/0969-8043(94)90190-2.
[9] P. Hettiarachchi, V. Cooray, M. Rahman, J. Dwyer, Energy Distribution of X-rays Produced by Meter-Long Negative Discharges in Air, Atmosphere 8 (2017) (2017) 244, https://doi.org/10.3390/atoms8120244.
[10] J.H. Hubbell, S.M. Seltzer, X-Ray Mass Attenuation Coefficients. NIST Standard Reference Database 126, https://www.nist.gov/pml/x-ray-mass-attenuation-coefficients (accessed August 17, 2020).
[11] S.M. Seltzer, M.J. Berger, Bremsstrahlung energy spectra from electrons with kinetic energy 1 keV-100 GeV incident on screened nuclei and orbital electrons of neutral atoms with $Z = 1$–100, At. Data Nucl. Data Tables 35 (1986) 345, https://doi.org/10.1016/0092-640x(86)90014-8.
[12] M.J. Berger, S.M. Seltzer, ESTAR: Stopping Powers and Ranges for Electrons, https://physics.nist.gov/PhysRefData/Star/Text/ESTAR.html (accessed October 17, 2020).
[13] H.B. Zhao, R. Carter, C.D. Hannaford, P. Zhou, E.A. Hughes, The improvement of the output performance of a low energy medical standing wave accelerator, Nucl. Instr. and Meth. in Phys. Res. A 356 (1995) 552–557, https://doi.org/10.1016/0168-9002(94)01248-2.